Journal of Sustainable Development of Energy, Water and Environment Systems

http://www.sdewes.org/jsdewes

Year 2026, Volume 14, Issue 3, 1140724

Original Research Article

Optimal Application of Pinch Power Analysis in Hybrid System Sizing and for Electric Vehicle Charging Stations

Bouthayna Slimani, Aboubekr Allam, Hassan Zahboune, Smail Zouggar[1], Mohamed.L. Elhafyani , Taoufik Ouchbel

University Mohammed 1, School of Technology, Laboratory of Electrical Engineering and Maintenance (LEEM). BP, 473, 60000 Oujda. Morocco

e-mail: bouthayna.slimani.d23@ump.ac.ma, aboubekr.allam@ump.ac.ma, H.zahboune@ump.ac.ma, smail.zouggar@ump.ac.ma, m.elhafyani@ump.ac.ma, t.ouchbel@ump.ac.ma

Cite as: Slimani, B., Allam, A., Zahboune, H., Zouggar, S., Elhafyani, M. L., Ouchbel, T., Optimal Application of Pinch Power Analysis in Hybrid System Sizing and for Electric Vehicle Charging Stations, J.sustain. dev. energy water environ. syst., 14(3), 1140724, 2026, DOI: https://doi.org/10.13044/j.sdewes.d14.0724

ABSTRACT

This study proposes an optimisation framework for the optimal sizing of a hybrid renewable energy system composed of photovoltaic generation, wind power generation, and a battery energy storage system. The system is governed by an energy management system integrating the Pinch Power Analysis method, and the results are validated using the Hybrid Optimization Model for Electric Renewables software. This framework is applied to a case study in the city of Oujda in Morocco, considering a residential electricity demand coupled with charging of electric vehicles. The results indicate that improving energy reliability requires higher installed generation and storage capacities. They show that the levelized cost of energy of the system composed of photovoltaic generation and battery energy storage (0.083 EUR/kWh) is lower than that of the configuration combining wind power generation, photovoltaic generation, and battery energy storage (≈ 0.10 EUR/kWh) for a loss of power supply probability below 2%. However, the integration of wind power reveals favourable temporal complementarity with photovoltaic generation. This complementarity significantly reduces storage requirements, stabilises battery state of charge cycles, and limits the deep discharges observed in the configuration composed only of photovoltaic generation and battery energy storage. The analysis is further extended through a sensitivity assessment of the electricity demand associated with electric vehicle charging, corresponding to 737 charging sessions per year with one charging station and 484 sessions per year with two charging stations. This increase in electricity demand raises the overall load while inducing only a limited impact on economic and reliability indicators, thereby confirming the ability of the system to adapt dynamically to variations in demand. In addition, surplus electricity production is exported to the grid, improving the economic viability of the studied systems.

KEYWORDS

Energy management system, Electric vehicle, Levelized cost of energy, Loss of power supply.

INTRODUCTION:

The sustained growth in electricity demand necessitates a transformation of energy systems to promote the integration of solar and wind power. However, the intermittency of these resources poses significant challenges to stability and reliability, making the deployment of hybrid renewable energy systems (HRES) coupled with storage technologies essential. Concurrently, the increasing integration of electric vehicles (EV) into microgrids introduces

new challenges related to the sizing and management of charging stations, requiring intelligent strategies to minimise costs and maximise energy efficiency.

From a systemic perspective, the literature highlights the diversity of hybrid configurations deployed to meet cost, reliability, and environmental assessment requirements, such as Life Cycle Assessment (LCA) within energy systems **[1].** Techno-economic evaluation primarily relies on indicators such as the levelized cost of energy (*LCOE*) and the loss of power supply probability (*LPSP*), applied to both grid-connected (on-grid) and autonomous (off-grid) architectures. Recent studies employ various optimisation approaches.

In off-grid PV/ battery energy storage (BESS) configurations, particle swarm optimisation (PSO), applied to a smart photovoltaic (PV) microgrid, achieves an *LPSP* of 0.18%, an *LCOE* of 0.0187 USD/kWh, and a renewable energy penetration rate of 98%, reflecting optimised power-flow management and reduced annualised costs **[2]**. In another approach, integrating battery/hydrogen storage, a comparison at *LPSP* = 1% shows that the total solar panel capacity of the PV/BESS system is 44.8% lower than that of the PV/hydrogen system **[3]**.

Hybrid systems incorporating thermal or hydraulic backup highlight additional trade-offs. Optimisation using the genetic algorithm (GA) for a PV/Diesel/PHS system results in an energy cost of 0.27 USD/kWh, which is lower than that of an optimised PV/Diesel/BESS reaching 0.34 USD/kWh **[4]**.

The integration of wind turbines (WT) represents an additional leverage, as analysed in several studies. For example, in an off-grid context in Kenya, a PV/WT/BESS–flywheel hybrid system modelled using MATLAB/Simulink and optimised with Multi-Objective Particle Swarm Optimisation (MOPSO) achieves an *LCOE* of 0.519 USD/kWh and an energy independence ratio (EISR) of 99.7% **[5]**. A WT/PV/hydrogen configuration optimised using a modified Non-dominated Sorting Genetic Algorithm II (NSGA-II) coupled with CRITIC-TOPSIS achieves an *LCOE* of 0.226 USD/kWh and an *LPSP* of 4.01% **[6]**.

In Bangladesh, a PV/WT/diesel/BESS optimised using GA-PSO with *LPSP* < 1% reaches a minimum *LCOE* of 0.234 USD/kWh, compared with 0.246 USD/kWh using PSO and 0.265 USD/kWh using GA. In addition, the valorisation of surplus energy reduces the total system cost by up to 11.8% and the electricity cost by 9.3% **[7]**. Consistently, the application of GA-PSO to a PV/WT/BESS system results in an *LCOE* of 0.502 USD/kWh for a maximum *LPSP* of 2%, corresponding to cost reductions of 42.17% compared with the WT/BESS system and 17.17% compared with the PV/BESS **[8]**.

In the hyper-arid region of Tamanrasset (Algeria), a study using MOPSO for the optimisation of an off-grid HRES integrating PV, WT, batteries, and a diesel generator reports an *LCOE* of 0.05433 USD/kWh, an *LPSP* of 3.1%, and a renewable fraction of 98%, demonstrating a strong capability to meet energy demand while maintaining high renewable integration. In comparison, simulations with Hybrid Optimisation of Multiple Energy Resources (HOMER Pro) software lead to an *LCOE* of 0.349 USD/kWh and a renewable fraction of 100%, illustrating that MOPSO provides a better trade-off between cost, reliability, and renewable integration **[9]**.

A recent study employing the differential optimization multiagent (DOMA) algorithm, with comparison to the Salp Swarm Algorithm (SSA) and the Whale Optimisation Algorithm (WOA) for optimising a microgrid in Najran, Saudi Arabia, shows that the PV/BESS system achieves the lowest *LCOE* (0.041 USD/kWh) but with limited reliability (*LPSP* = 0.6723%), while the PV/WT/BESS configuration provides a better compromise between cost and reliability (*LCOE* = 0.098 USD/kWh, *LPSP* = 0.3129%) **[10]**.

The distinction between off-grid and grid-connected systems is explicitly highlighted in the analysis of a commercial building optimised using HOMER Pro. In the first on-grid scenario, supplied by WT energy and the grid, the *LCOE* is 0.0976 USD/kWh, with renewable penetration and *LPSP* rates of 23.3% and 76.7%, respectively. The second scenario, based on solar energy and the grid, presents an *LCOE* of 0.111 USD/kWh, with a renewable penetration of 66.6% and an *LPSP* of 34%. The third scenario, combining PV/WT/grid, results in an *LCOE*

of 0.1083 USD/kWh, with renewable penetration and *LPSP* values of 64.9% and 35.1%, respectively. These results show that WT energy, although presenting the lowest *LCOE*, is not sufficient to fully satisfy demand when used alone [11].

A study integrating real climatic and load data for grid-connected HRES, including PV, WT, and a BESS, shows that the reliability constraint (LPSP) strongly influences the LCOE depending on the optimisation methods applied: Moth-Flame Optimisation Algorithm (MFOA), Whale Optimisation Algorithm (WOA), Flower Pollination Algorithm (FPA), GA. For example, for an *LPSP* of 0.5%, the *LCOE* is 0.1443 USD/kWh, gradually decreasing to 0.1342 USD/kWh for an *LPSP* of 10%. Simulation results indicate that the PV/WT/BT configuration represents the most cost-effective and reliable option, with an *LCOE* of 0.1342 USD/kWh, corresponding to a cost reduction of 33% compared with an off-grid configuration [12].

Moreover, the Electric System Cascade Extended Analysis (ESCEA) tool enables the determination of the optimal sizes of renewable energy installations for both grid-connected and standalone configurations, assuming a reduced *LPSP*.

Results reported in the literature indicate that the *LCOE* varies depending on the system configuration. For standalone systems, an *LCOE* of 0.21 USD/kWh has been obtained for a PV/BESS system [13], while an *LCOE* of 0.196 USD/kWh has been reported for a CSP/TES system [14]. For grid-connected configurations, the reported *LCOE* values are 0.225 USD/kWh for WT, 0.110 USD/kWh for PV [15] , and 0.210 USD/kWh for a CSP system without thermal storage [16] . Furthermore, for an isolated power supply system composed of PV/WT/BESS, previous studies have reported *LCOE* values of 0.3747 EUR/kWh [17]. In addition, the results presented in [18] indicate that it is possible to achieve an *LCOE* of 0.25 EUR/kWh under specific operating conditions.

In the context of EV integration, several studies have proposed optimisation approaches aimed at improving both the cost and reliability of energy systems. Study [19] employs a two-stage multi-objective stochastic programming approach for an isolated microgrid, showing that a trade-off between *LPSP* and cost can reduce expenses by 10–20%. Meanwhile, [20] applies a multi-objective whale optimisation algorithm (MOWOA) to optimally size PV, WT, BESS, and EV charging infrastructure, maximising energy efficiency and self-consumption while minimising total cost. In addition, [21] introduces an indicator to evaluate the balance between self-consumption and self-sufficiency.

Furthermore, studies such as [22] and [23] focus on the techno-economic modelling of charging stations under grid-connected or hybrid configurations. Study [22] proposes Python-based models for PV/grid and PV/grid/BESS systems and highlights the use of HOMER Grid to simulate and analyse load profiles. It particularly emphasises the flexibility of this tool in modelling a charging station of 150 EVs (maximum charging power of 85 kW, 7,253 charging sessions per year, 207,211 kWh/year), enabling the assessment of the impact of the number of chargers on system availability and techno-economic performance.

Similarly, [23] uses HOMER software with NASA-derived data to analyse two sites. For one site, the optimal energy configuration consists of a PV system, batteries, a wind turbine, and a converter, with an *LCOE* of 0.450 USD/kWh.

Finally, smart EV charging management is addressed in [24] and [25]. Study [24], based on the OCHRE tool integrated into a Home Energy Management System (HEMS), demonstrates a 23% reduction in peak demand through optimised charging. Study [25] proposes a real-time energy management strategy coordinating grid-connected PV and BESS.

Overall, these approaches converge with recent research showing that optimising HRES integrating PV, biomass, and fuel cells in the presence of EVs significantly improves overall system performance. In a scenario without EV charging, the MCWOA achieves an *LCOE* of 0.2273 USD/kWh and an *LPSP* of 2.349%, whereas integrating EV charging demand reduces the *LCOE* to 0.2203 USD/kWh while maintaining a high level of reliability (*LPSP* = 2.209%) [26].

This study develops an optimisation framework aimed at the optimal sizing of a hybrid system combining PV, WT, and BESS, managed by an energy management system (EMS) integrating the Pinch Power Analysis method. The adopted methodology is structured into several complementary and sequential steps:

- Generation of EV charging profiles.
- Energy modelling of system components, including PV and WT generation, BESS, and residential load with EV charging. This step is organised into two steps:
  - Daily-based preliminary sizing and energy balance optimisation to establish a preliminary system configuration.
  - Hourly-based annual verification with operational constraints, enabling precise evaluation of the sizing over the full 8760 h annual horizon with a one-hour timestep.
- Definition of technical constraints, such as the minimum and maximum BESS state-of-charge levels and power limits, along with the assessment of key economic and reliability performance indicators.
- Implementation of the Energy Management System (EMS) based on Pinch Power Analysis, to optimise energy flow management and reduce imbalances between production and demand.
- Sensitivity analysis on EV charging demand, performed after generating the charging profiles, to evaluate system robustness under varying usage patterns and progressively increasing energy requirements.
- Validation of results through comparison with HOMER software, in the context of a case study applied to the city of Oujda (Morocco), ensuring the consistency and reliability of the optimised configurations.

System Modelling

The HRES combines PV panels, WT turbines, and BESS to power residential loads and recharge EVs. The different components of this system are modelled as follows:

Photovoltaic panel model. A PV model allows analysis of variations in efficiency and performance, which decrease as temperature increases, to maximise energy production.

The output power produced by PV system depends on the specific characteristics of the PV array and the solar irradiance received, and can be calculated using eq. (1):

$$P\mathrm{pv}\,(t) \;=\; P_{\mathrm{rated}} \times \frac{G(t)}{G_{\mathrm{T,STC}}} \times [1 - \beta \times (T_{\mathrm{c}}(t) - T_{\mathrm{ref}})] \tag{1}$$

where are: p_{rated}- the rated capacity of the PV array, meaning its power output under standard test conditions [kW]; $G(t)$- the solar radiation incident on the PV array in the current time step [kW/m^2]; $G_{\mathrm{T,STC}}$- the incident radiation at standard test conditions [1 kW/m^2]; β- the temperature coefficient of power [%/°C]; $T_{\mathrm{c}}(t)$- the PV cell temperature in the current time step [°C]; T_{ref}- the PV cell temperature under standard test conditions [25 °C].

Wind turbine model. The wind turbine model converts wind energy into electrical power based on wind speed, which must be adjusted to the turbine hub height for accurate estimation.

Calculating Hub Height Wind Speed. is calculated from the wind speed measured at the anemometer height by applying the power law eq. (2):

$$V_{\mathrm{hub}}(t) \;=\; V_{\mathrm{anem}}(t) \times \left(\frac{H_{\mathrm{hub}}}{H_{\mathrm{anem}}}\right)^{\alpha} \tag{2}$$

where are: $V_{\text{hub}}(t)$ - the wind speed at the hub height of the wind turbine [m/s]; $V_{\text{anem}}(t)$ - the wind speed at anemometer height [m/s]; H_{hub}- the hub height of the wind turbine [m]; H_{anem}- the anemometer height [m]; α- the power law exponent [-].

Calculation of wind turbine electrical power. The electrical power produced ($P_{\text{WTG,STP}}(t)$) is derived from the standardised wind power curve (**Figure 1**):

If $V_{\text{hub}}(t)$ is outside the operating range of the curve (below the minimum rated wind speed or above the cut-out wind speed), the power is zero:

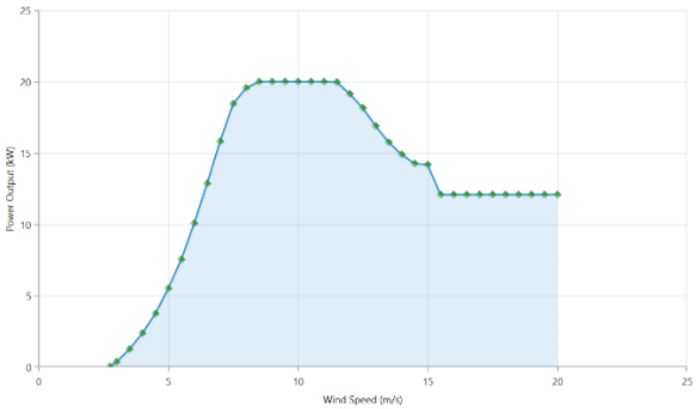

Figure 1. Wind turbine power curve

The actual power produced is adjusted according to the real air density relative to the standard air density (standard temperature and pressure conditions):

$$P_{\text{WTG}}(t) = \left(\frac{\rho}{\rho_0}\right) P_{\text{WTG,STP}}(t) \times \eta_{\text{gearbox}} \times \eta_{\text{generator}} \quad (3)$$

where are: ρ - teal air density [kg/m³]; ρ_0 - standard air density [1.225 kg/m³]; η_{gearbox} - the efficiency of the multiplier [%]; $\eta_{\text{generator}}$- the efficiency of the generator [%].

Energy Storage System Model

The BESS is an essential component of the proposed energy system, ensuring operational flexibility and supply reliability. The EMS coordinates charging and discharging to enhance system reliability while maximising the utilisation of available energy resources.

To accurately represent the dynamic behaviour of the BESS, key parameters such as energy capacity and state of charge (*SOC*) are considered eq. (4), it is constrained within predefined lower and upper bounds, to ensure safe and efficient operation:

$$SOC_{\text{BESS}}(t) = \frac{E_{\text{acc}}(t)}{C_{\text{BESS}}} \quad (4)$$

where are: $E_{\text{acc}}(t)$- the energy stored at time *t*; C_{BESS}- the total BESS capacity, representing the maximum amount of energy it can store [kWh]; $SOC_{\text{BESS}}^{\min}$- minimum allowable state of charge of the BESS [%]; $SOC_{\text{BESS}}^{\max}$: maximum allowable state of charge of the BESS [%].

BESS sizing is performed by considering the depth of discharge (DOD), which limits the usable portion of C_{BESS} to prolong battery lifetime and maintain system stability. Accordingly, the effective or net storage capacity of the BESS is given by eq. (5):

$$C_{\text{net}} = \frac{(E_{\text{acc}}^{\max} - E_{\text{acc}}^{\min})}{DOD} \text{ [kWh]} \quad (5)$$

where are: $E_{\text{acc}}^{\max}$- the maximum accumulated energy in the BESS over the period T; $E_{\text{acc}}^{\min}$- the minimum accumulated energy in the BESS over the period *T*.
Based on the required net capacity, the total number of batteries needed in the BESS is calculated as eq. (6):

$$N_{\text{bat}} = \frac{C\text{net}}{C_{\text{BESS}}} \quad (6)$$

Model of Electric Vehicle

The EV modelling framework aims to simulate the energy needs for charging by incorporating user behaviours (arrival and departure times, distances travelled, parking habits) alongside vehicle characteristics, energy consumption, and charging strategies:

Number of electric vehicles. Number of EVs (N_{EV}) is essential to specify the number of EVs present at the station.

Optimal number of chargers. The charging station is equipped with an optimal number of chargers N_{stat}, determined based on the cumulative charging demand and the total time required to serve planned charging events.

Energy consumption per kilometre. Energy consumption per kilometre ($E_{\text{km}}^{\text{ID}}$) value typically ranges between 0.15 and 0.18 kWh/km, depending on the vehicle model (**Table 11**).

Battery capacity of electric vehicle. Each vehicle has a specific battery capacity *($Cbat_{\text{EV}}^{\text{ID}}$)* (in kWh) (**Table 11**).

Maximum charging power provided by the charger. Each charger delivers a maximum charging power ($Charg_{\text{pow}}^{\max}$) (in kW), corresponding, for example, 1.4 kW for Level 1 charging or 9 kW for Level 2 charging **[22]**.

Maximum charging power accepted by EV. The maximum power ($Charg_{\text{pow\_EV}}^{\max}$) that the vehicle can accept during charging (**Table 11**).

Smart Charging control. At any time, the EV can be in one of three states:

- Connected and charging
- Connected but waiting for charger availability,
- Disconnected (no charging).

These states allow modelling charger occupancy, queuing effects, and waiting times without invoking control or optimisation logic.

The target state of charge. for each EV eq. (7) is defined based on the recovered driving range required after charging, and is expressed as:

$$SOC_{\text{target}}^{\text{ID}_{\text{EV}}} = SOC_{\min}^{\text{ID}_{\text{EV}}} + \frac{RDR_{\text{target}}^{\text{ID}_{\text{EV}}} \times E_{\text{km}}^{\text{ID}_{\text{EV}}}}{Cbat_{\text{EV}}^{\text{ID}_{\text{EV}}}} \quad (7)$$

where are: $SOC_{\min}^{\mathrm{ID_{EV}}}$- minimum *SOC* of the EV battery [%]; $SOC_{\mathrm{target}}^{\mathrm{ID_{EV}}}$ – the target SOC that the EV battery aims to reach [%]; $RDR_{\mathrm{target}}^{\mathrm{ID_{EV}}}$ –target recovered driving range, defined as the distance that the vehicle intends to cover after a recharge [km] (**Table 11**).

The charging duration. depends on the requested energy and charger availability. Two charging modes are modelled:

- Partial (requested) charging: when full charging cannot be completed due to time or station constraints in (minutes):

$$\Delta t_{partial} = \frac{\left(SOC_{\mathrm{target}}^{\mathrm{ID_{EV}}} - SOC_{\mathrm{initial}}^{\mathrm{ID_{EV},}Day}\right) \times Cbat_{\mathrm{EV}}^{\mathrm{ID_{EV}}} \times 60}{\min\left(Charg_{\mathrm{pow}}^{\max}, Charg_{\mathrm{pow\_EV}}^{\max}\right)} \quad (8)$$

- Full charging: when sufficient time and charger availability are ensured in (minutes):

$$\Delta t_{\mathrm{full}} = \frac{\left(SOC_{\mathrm{max}}^{\mathrm{ID_{EV}}} - SOC_{\mathrm{initial}}^{\mathrm{ID_{EV},}Day}\right) \times Cbat_{\mathrm{EV}}^{\mathrm{ID_{EV}}} \times 60}{\min\left(Charg_{\mathrm{pow}}^{\max}, Charg_{\mathrm{pow\_EV}}^{\max}\right)} \quad (9)$$

where: $SOC_{\mathrm{max}}^{\mathrm{ID_{EV}}}$- maximum *SOC* of the EV battery [%].

Initial state of charge of EV batteries. The *SOC* upon arrival on the following day is updated depending on whether charging has occurred:

With charging:

$$SOC_{\mathrm{initial}}^{\mathrm{ID_{EV},Day+1}} = \max\{[\,SOC_{\mathrm{initial}}^{\mathrm{ID_{EV},}Day} + \frac{\Delta t \times \min\left(Charg_{\mathrm{pow}}^{\max}, Charg_{\mathrm{pow\_EV}}^{\max}\right)}{60 \times Cbat_{\mathrm{EV}}^{\mathrm{ID_{EV}}}} - (SOC_{\mathrm{target}}^{\mathrm{ID_{EV}}} - SOC_{\mathrm{min}}^{\mathrm{ID_{EV}}})], SOC_{\mathrm{min}}^{\mathrm{ID_{EV}}}\} \quad (10)$$

Without charging:

$$SOC_{\mathrm{initial}}^{\mathrm{ID}_{EV},\mathrm{Day+1}} = max\{[SOC_{\mathrm{initial}}^{\mathrm{ID},Day} - (SOC_{\mathrm{target}}^{\mathrm{ID_{EV}}} - SOC_{\mathrm{min}}^{\mathrm{ID_{EV}}})\,],\ SOC_{\mathrm{min}}^{\mathrm{ID_{EV}}}\} \quad (11)$$

MATERIALS AND METHODS

This study proposes a methodology for generating EV load profiles to simulate the energy consumption of charging stations while optimising the available energy resources (**Figure 2**). The simulation process includes determining the optimal number of charging stations, generating the EV load profile, and using it to adjust energy resources through Pinch Power Analysis and EMS. This approach enables the resizing of renewable energy production (PV and WT) and BESS within an HRES, while relying on the techno-economic constraints that will be identified, to balance production and consumption, ensuring optimal resource management, thereby guaranteeing the performance and sustainability of the BESS.

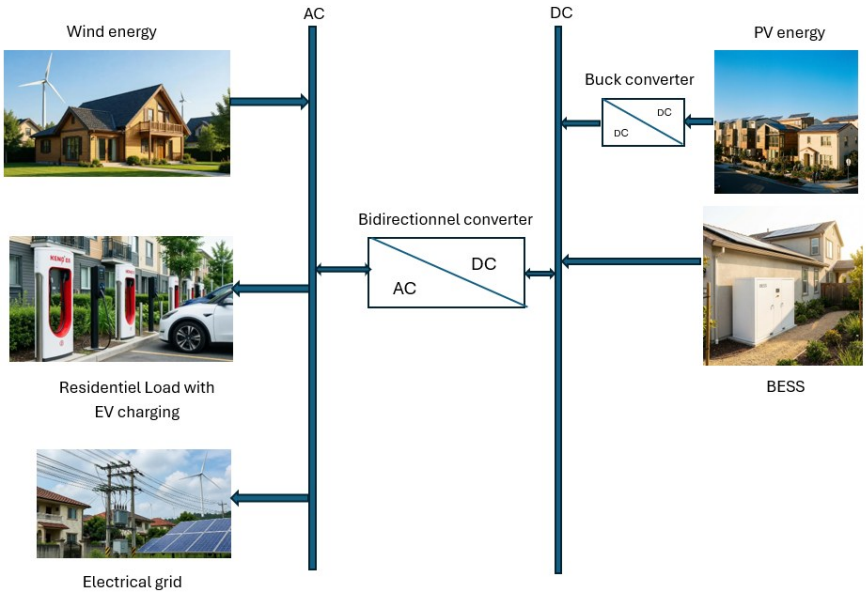

Figure 2. Flow Diagram between Renewable Sources, BESS, and Loads

Electric Vehicle Load Profile Generation

Based on the previously defined EV modelling framework, a method is developed to determine the optimal number of charging stations and generate the EV charging load profile over an annual simulation horizon. The process follows the algorithm illustrated in (**Figure 3**) and operates on a day-by-day and vehicle-by-vehicle basis.

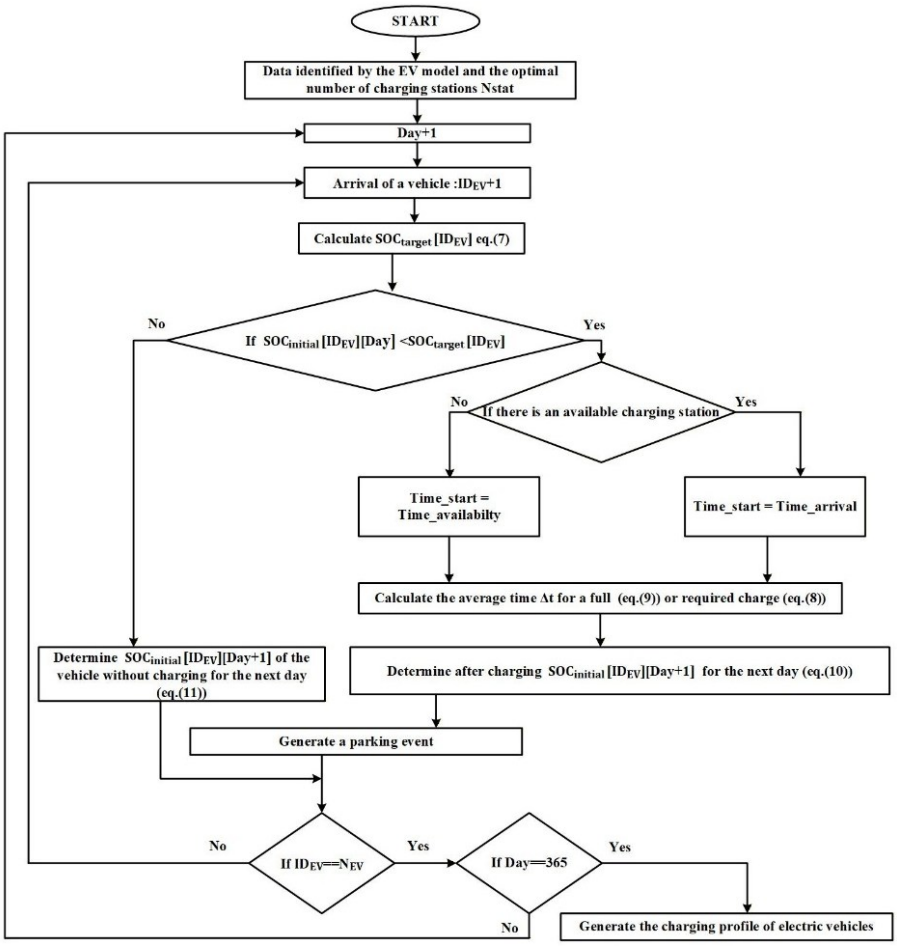

Figure 3. Flowchart of consumption profile generation for EV charging

When an EV arrives:

- Its $SOC_{\text{initial}}^{\text{ID,Day}}$ is compared with $SOC_{\text{target}}^{\text{ID,Day}}$
- If the $SOC_{\text{initial}}^{\text{ID,Day}}$ is sufficient, no charging action is scheduled.
- Otherwise, charger availability is evaluated:
  - If a charger is available, charging starts immediately: $t_{\text{start}} = t_{\text{arrival}}$
  - If no charger is available, charging is delayed until the first charger becomes available: $t_{\text{start}} = t_{\text{availability}}$

A smart charging scheme is adopted, where charging does not necessarily start immediately upon connection, nor does it always operate at maximum power. Instead, charging power and timing are adjusted based on charger occupancy and remaining parking duration:

- Full charging is prioritised when feasible.
- Partial charging is applied when time constraints (t_{depart} : departure time) exist or when other EVs are waiting for a charging point to become available, thereby preventing full charging.

The average charging duration is determined using eqs. (8) and (9), ensuring compatibility with infrastructure and user requirements.

At the end of each charging session, a parking event is recorded, including:

- Arrival $SOC_{\text{initial}}^{\text{ID,Day}}$,
- Charging Start/End time,
- Charging duration,
- Energy delivered.

The next EV arrival is then processed until all EVs of the day are served. This procedure is repeated daily until the end of the year (Day=365).

The aggregation of all recorded charging events results in the annual EV charging profile.

Optimisation Constraints

The optimisation of HRES and BESS relies on constraints and key indicators that influence their performance, profitability, and management, particularly in the face of the intermittency of solar and WT sources. Among the main evaluation criteria considered in this study, the following have been identified:

Final Excess Energ. (*FEE*) is the difference between the energy accumulated in the BESS at the end and the beginning of the analysis period. It represents the surplus energy in the system after meeting all demands, and is given by:

$$FEE = SOC_{\text{BESS}}(t) - SOC_{\text{BESS}}(t = 0) \quad (12)$$

If $FEE < 0$, the BESS charging leads to failure.
If $FEE > 0$ => the charging of the BESS explains an over-sizing of the energy components.

Loss of Power Supply Probability. represents the ratio between the total of energy not satisfied eq. (26) and the total energy demand over the analysis period in:

$$LPSP = \frac{\sum_{t=0}^{t=8759} LPS(t) \times \eta_{\text{DC/AC}} \times \eta_{\text{disch}}}{\sum_{t=0}^{t=8759} E_{\text{Load}}(t)} \quad (13)$$

Excess power supply probability. quantifies the portion of renewable energy that cannot beutilized due to generation exceeding both load demand eq. (23) and the total energy generated (eq. (17) and eq. (18)) over the analysis period. It reflects the effectiveness of the EMS in utilising available renewable resources, and is given by:

$$EPSP = \frac{\sum_{t=0}^{t=8759} EPS(t)}{\sum_{t=0}^{t=8759} Epv\_wind(t) \times \eta_{\text{ch}} \times \eta_{\text{AC/DC}}} \quad (14)$$

Levelized Cost of Energy. *LCOE* is an economic indicator used to evaluate the average cost of generating one unit of energy over the lifetime of a production system, given by:

$$LCOE = \frac{(cost_{\text{comp}} + cost_{\text{installation}} + cost_{\text{BOS}}) \times CRF + cost_{\text{M\&O}}}{\sum_{t=0}^{t=8759} E_{\text{Load}}(t)} \quad (15)$$

where are: $cost_{\text{comp}}$- the purchase cost of all required equipment [EUR]; $cost_{\text{installation}}(t)$: the installation cost [EUR]; $cost_{\text{BOS}}$- the balance of system cost [EUR]; $cost_{\text{M\&O}}$- the operation and maintenance cost [EUR].

CRF is the capital recovery factor and is computed as:

$$CRF = \frac{r \times (1+r)^L}{(1+r)^L - 1} \quad (16)$$

where are: r - the interest rate; L - the lifetime.

Energy Generation Ratio. Energy Generation Ratio (*EGR*) represents the relative distribution of energy production between PV by eq. (17) and WT sources by eq. (18) in HRES:

$$\sum_{\text{t=0}}^{\text{t=24}} Epv(\text{t}) \times Npv = \frac{EGR \times \sum_{t=0}^{t=24} Epv\_wind(t)}{\eta_{\text{DC/DC}} \times \eta_{\text{DC/AC}}} \quad (17)$$

and:

$$\sum_{t=0}^{t=24} Ew(t) \times Nw = (1 - EGR) \times \sum_{t=0}^{t=24} Epv\_wind(t) \quad (18)$$

where are: $Epv\_wind(t)$- the total energy produced by the renewable sources; $Epv(t)$- the energy produced by a single PV; $Ew(t)$ - the energy produced by a single WT; Npv - the number of installed PV panels; Nw- the number of installed WT; $\eta_{\text{DC/DC}}$: correspond to the efficiencies of the DC/DC conversion stage; $\eta_{\text{DC/AC}}$: correspond to the efficiencies of the AC/DC conversion stage.

Battery Energy Charging Ratio. Ratio of discharged to charged energy in the BESS over a given period (*BECR*) in:

$$BECR = \frac{\sum_{t=0}^{t=24} \left| E_{\text{BESS}}^{\text{disch}}(t) \right|}{\sum_{t=0}^{t=24} E_{\text{BESS}}^{\text{ch}}(t)} \quad (19)$$

Energy Management Strategy

The primary function of the Energy Management System (EMS) is to coordinate energy generation, consumption, and BESS to ensure supply reliability, maximise renewable energy utilisation, and minimise dependency on the utility grid.

Operational strategy for energy management. The EMS implements a priority-based strategy to maximise renewable energy utilisation, maintain system reliability, and optimise battery operation. The operational strategy is structured as follows:

- Battery Charging Mode: ($Epv\_wind(t)$>$E_{\text{Load}}(t)$):
  - Case 1: Wind production covering the demand: If the wind production satisfies the demand ($Ew(t)$≥$E_{\text{Load}}(t)$):
    Then the residual energy is expressed as:

$$Er(t) = (Ew(t) \times Nw - E_{\text{Load}}(t)) \times \eta_{\text{AC/DC}} + Epv(t) \times Npv \times \eta_{\text{DC/DC}} \quad (20)$$

  - Case 2: PV + WT production covering the demand: If the wind production is insufficient but the combined PV and wind production meets the demand ($Ew(t)$<$E_{\text{Load}}(t)$):
    Then the residual energy is:

$$Er(t) = \frac{Epv\_wind(t) - E_{\text{Load}}(t)}{\eta_{\text{AC/DC}}} \quad (21)$$

The battery charges if its *SOC* satisfies ($SOC_{\text{BESS}}(t) < SOC_{\text{BESS}}^{\max}$ with the charging power limited by:

$$E_{\text{BESS}}^{\text{ch}}(t) = \min\{Er(t) \times \eta_{\text{ch}}, E_{\text{acc}}^{\max} - E_{\text{acc}}(t-1)\} \quad (22)$$

When the battery reaches its maximum capacity $SOC_{\text{BESS}}^{\max}$, it no longer charges. The excess energy is exported to the grid by [7][26]:

$$EPS(t) = \max\left\{\frac{E_{\text{acc}}(t) - E_{\text{acc}}^{\max}}{\eta_{\text{AC/DC}} \times \eta_{\text{ch}}}, 0\right\} \quad (23)$$

- Battery Discharging Mode:
  - Case 3: Renewable production below demand: If renewable production is less than the demand ($Epv\_wind(t) < E_{\text{Load}}(t)$) and the SOC_{BESS} is below the minimum allowed level $SOC_{\text{BESS}}(t) < SOC_{\text{BESS}}^{min}$, the battery discharges to compensate the energy deficit according to:

$$E_{\text{BESS}}^{\text{disch}}(t) = \min\left\{\frac{Er(t)}{\eta_{\text{disch}}}, E_{\text{acc}}^{\min} - E_{\text{acc}}(t-1)\right\} \quad (24)$$

with residual energy calculated by:

$$Er(t) = \frac{Epv\_wind(t) - E_{\text{Load}}(t)}{\eta_{\text{DC/AC}}} \quad (25)$$

If the battery reaches the minimum threshold SOC_{BESS}^{min}, it ceases discharging and the uncovered deficit is expressed by:

$$LPS(t) = \max\left\{\frac{E_{\text{acc}}^{\min} - E_{\text{acc}}(t)}{\eta_{\text{DC/AC}} \times \eta_{\text{disch}}}, 0\right\} \quad (26)$$

Battery Energy Update. The energy stored in the BESS is updated at each time step according to the net charging or discharging action determined by the EMS in:

$$E_{\text{acc}}(t) = E_{\text{acc}}(t-1) + E_{\text{BESS}}^{\text{ch}}(t) + E_{\text{BESS}}^{\text{disch}}(t) \quad (27)$$

Pinch Power Analysis and Energy Management

This study proposes a structured, multi-stage optimisation framework developed in Python to determine the optimal configuration of a HRES composed of PV units, WT, and BESS, operated under an integrated EMS. The primary objective of the proposed optimisation framework is to identify the most suitable system sizing that minimises grid dependency while enhancing techno-economic and reliability performance indicators.

The methodology integrates meteorological inputs (solar irradiation, ambient temperature, and wind speed), residential load profiles, and EV charging demand over a one-year horizon (8760 h). The overall optimisation process is depicted as a step-by-step flowchart and follows a two-level sizing and verification strategy, inspired by Pinch Power Analysis concepts applied to EMS (**Figure 4**).

Step 1: Daily-Based Preliminary Sizing and Energy Balance Optimisation. In the first stage, all input data are aggregated into 24h daily average profiles to reduce computational complexity and enable a preliminary sizing of the generation and storage components. The optimisation process is initialised by setting the number of PV panels and WT to unity (*Npv*=*Nw*=1). At this stage, the EMS is executed without enforcing the $SOC_{\text{BESS}}^{\min}$ and $SOC_{\text{BESS}}^{\max}$, as the objective is to determine these suitable bounds for the BESS, which will be implemented in the second stage of the process.

The system performance (**Figure 4**), is evaluated through objective indicators, particularly *BECR* and *FEE*. Based on the *BECR* value, three resizing scenarios are considered to adjust the total amount of renewable energy to be produced:

- **Scenario 1 (*BECR* > 1):** When discharged energy exceeds charged energy, an additional amount of renewable energy is supplied to compensate for the deficit:

$$\sum_{t=0}^{t=24} E_{\text{pv}_{\text{wind}}}(t) = \sum_{t=0}^{t=24} E_{\text{pv}_{\text{wind}}}(t) + \left(\left|\sum_{t=0}^{t=24} E_{\text{BESS}}^{\text{disch}}(t)\right| - \sum_{t=0}^{t=24} E_{\text{BESS}}^{\text{ch}}(t)\right) \times \eta_{disch} \quad (28)$$

- **Scenario 2 (*BECR* < 1):** When charged energy exceeds discharged energy, the renewable generation capacity is curtailed accordingly:

$$\sum_{t=0}^{t=24} E_{\text{pv}_{\text{wind}}}(t) = \sum_{t=0}^{t=24} E_{\text{pv}_{\text{wind}}}(t) - \frac{\left(\sum_{t=0}^{t=24} E_{\text{BESS}}^{\text{ch}}(t) - \left|\sum_{t=0}^{t=24} E_{\text{BESS}}^{\text{disch}}(t)\right|\right)}{\eta_{\text{ch}} \times \eta_{\frac{\text{AC}}{\text{DC}}}} \quad (29)$$

- **Scenario 3 (*BECR* = 1):** Energy balance is achieved, and the sizing is considered optimal.

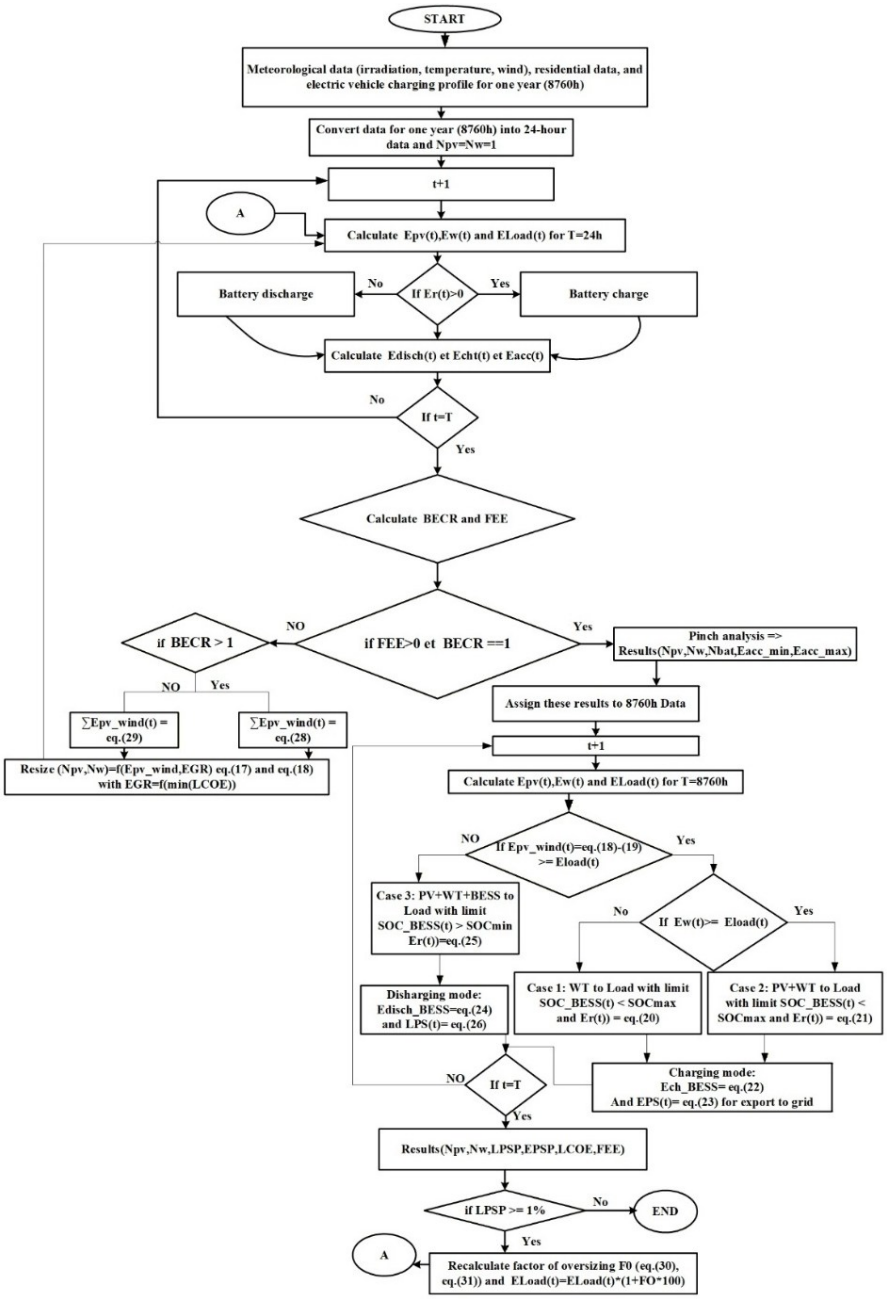

Figure 4. Flowchart of Pinch Power Analysis and EMS

Once equilibrium is achieved, a pinch analysis is applied by imposing $E_{\mathrm{acc}}^{\mathrm{initial}}$, ensuring strictly positive energy values throughout the analysis. This enables the determination of the minimum and maximum BESS energy limits, $E_{\mathrm{BESS}}^{\mathrm{min}}$ and $E_{\mathrm{BESS}}^{\mathrm{max}}$ which define the exploitable storage range, defined as eq. (5). These energy limits directly correspond to the operational limits of the SOC_{BESS}, set at 10% for discharge and 90% for charge. In addition, the optimal allocation between PV and wind generation is established through the *EGR*, chosen to minimise *LCOE*.

Step 2: Hourly-Based Annual Verification with Operational Constraints. The second stage performs a detailed verification of the sizing results obtained in Step 1 using the full 8760 h dataset with a one-hour timestep. During this phase, the integrated EMS is executed under strict operational constraints, including the previously defined $SOC_{\mathrm{BESS}}^{\mathrm{min}}$ and $SOC_{\mathrm{BESS}}^{\mathrm{max}}$, enabling the evaluation of key reliability indicators such as *LPSP* and the *EPSP*.

However, the use of daily average profiles in Step 1 may underestimate peak demand variations, potentially leading to an elevated *LPSP* during the annual assessment. To overcome this limitation, a load oversizing factor is iteratively applied only to the 24 h aggregated load profiles during Step 1, while the annual 8760 h dataset used in Step 2 remains unaltered to ensure realistic operational validation (**Figure 4**):

The oversizing factor is computed using a linear formulation when LPSP is high eq. (30):

$$FO = \frac{LPSP}{1 - LPSP} \ [\%] \tag{30}$$

and a logarithmic formulation when *LPSP* is below 5%:

$$FO = \frac{\ln (LPSP - 1\%)}{\ln (LPSP)} - 1 \tag{31}$$

The two-step procedure is repeated iteratively by adjusting the oversizing factor until the *LPSP* >1%, resulting in a more conservative and robust system sizing that significantly reduces *LPSP* during long-term operation.

Results and Discussion

This section presents all the results obtained within the framework of the case study conducted in the city of Oujda (Morocco), it is based on the collection and utilisation of data to provide a solid foundation for establishing demand scenarios intended for the optimal sizing of two hybrid energy production and storage configurations:

- **Configuration I:** PV and BESS
- **Configuration II:** PV, WT, and BESS

Local meteorological data (solar irradiation, temperature (**Figure 5**), and wind speed (**Figure 6**) were collected to characterise the climatic conditions specific to the region, and in addition, a charging profile for a fleet of 15 EVs was simulated and integrated into the existing residential load profiles, thus generating a comprehensive dataset that combines domestic consumption with specific mobility-related energy needs.

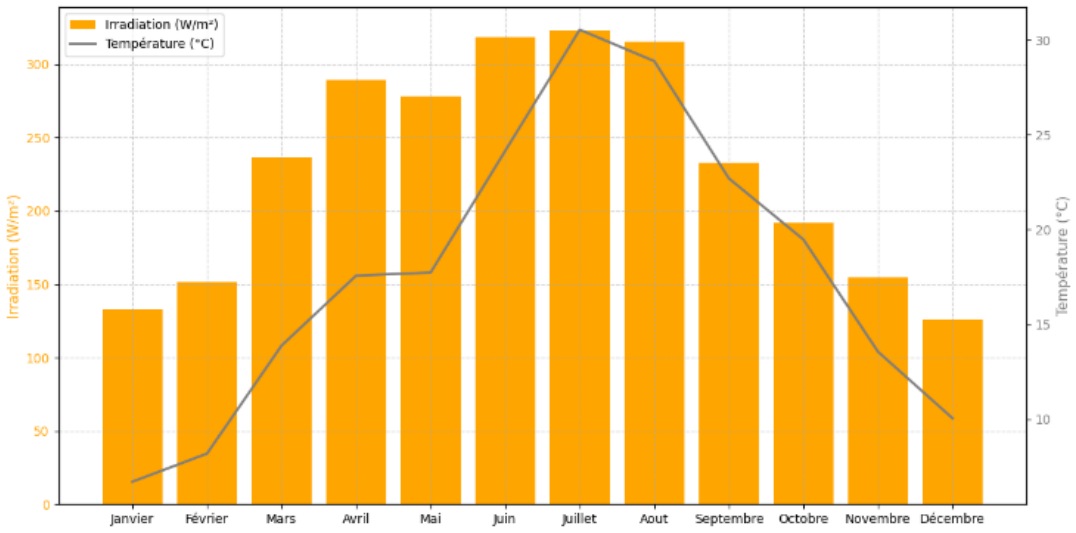

Figure 5. Monthly Variation of Solar Irradiance and Average Temperature (°C)

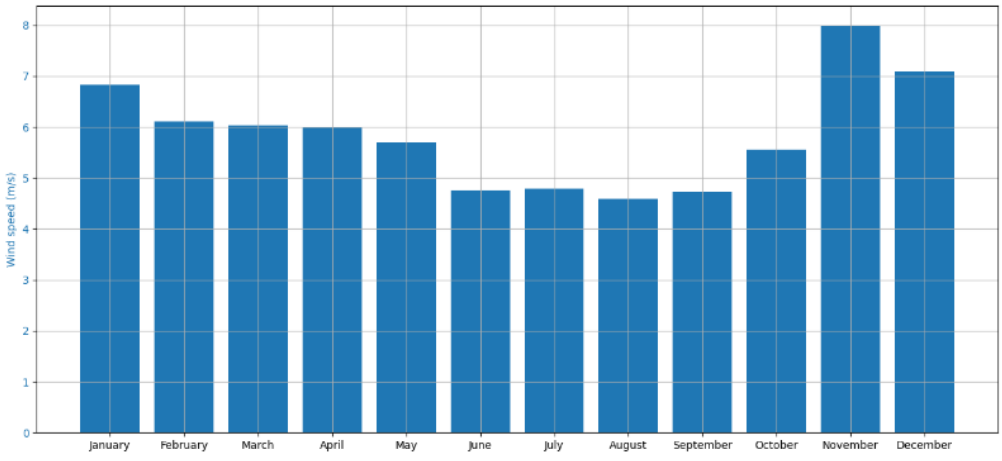

Figure 6. Monthly Average Wind Speed Variation (m/s) Throughout the Year

Electric Vehicle Charging Profile

The EV charging profile was established from data collected on 15 vehicles using Level 2 charging with $Charg_{pow}^{max}$ =11kW, and an analysis of charging habits reveals that the majority of vehicles are connected for charging in the late afternoon and evening, specifically between 16:00 and 23:30 (Appendix: **Table 11**), moreover, the batteries of the studied EVs have capacities ranging from 32.3 kWh to 64.8 kWh, with accepted charging powers generally between 7.2 kW and 7.4 kW. Furthermore, a simulation over a full year enabled the evaluation of the total number of charging sessions together with the associated satisfaction rate. In addition, the charging management analysis indicated that using either one or two chargers was feasible, which consequently led to the study of two cases: the first corresponds to the operation of a single charging station, while the second considers two stations operating simultaneously; these configurations represent the optimal solutions identified to meet the charging needs. To assess system performance, three performance indicators were selected, namely Maximum Satisfaction (vehicles fully charged), Required Satisfaction (vehicles reaching a minimum acceptable charge level), and the case where vehicles remain uncharged. As a result, the findings demonstrate that with two charging stations, overall satisfaction increases significantly, thereby reducing the number of undercharged vehicles. Finally, over the course of the year, 737 charging sessions were recorded for the first case (**Figure 7**) compared to 484 for the second case (**Figure 8**), suggesting that the choice between these two options ultimately depends on the trade-off between investment cost and the level of service provided.

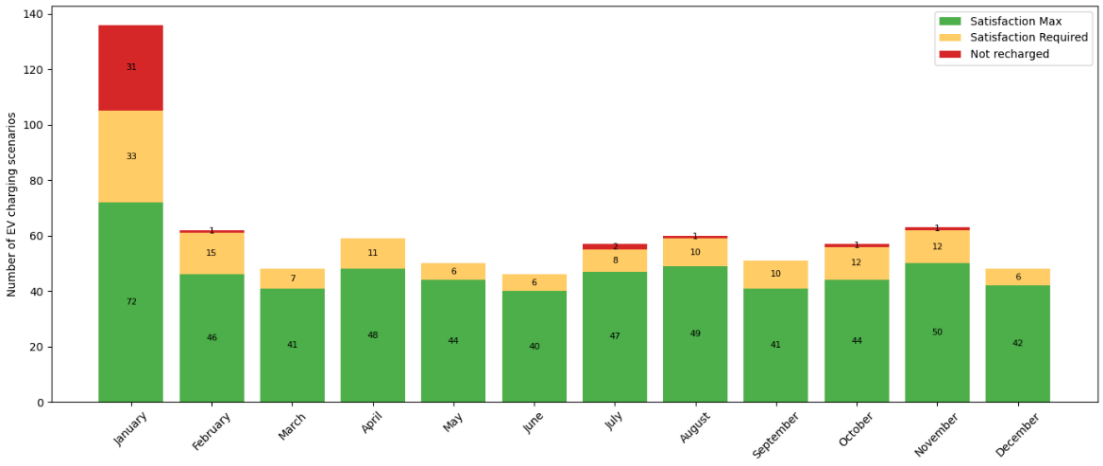

Figure 7. Charging sessions of EVs with the satisfaction rate for a single charging station

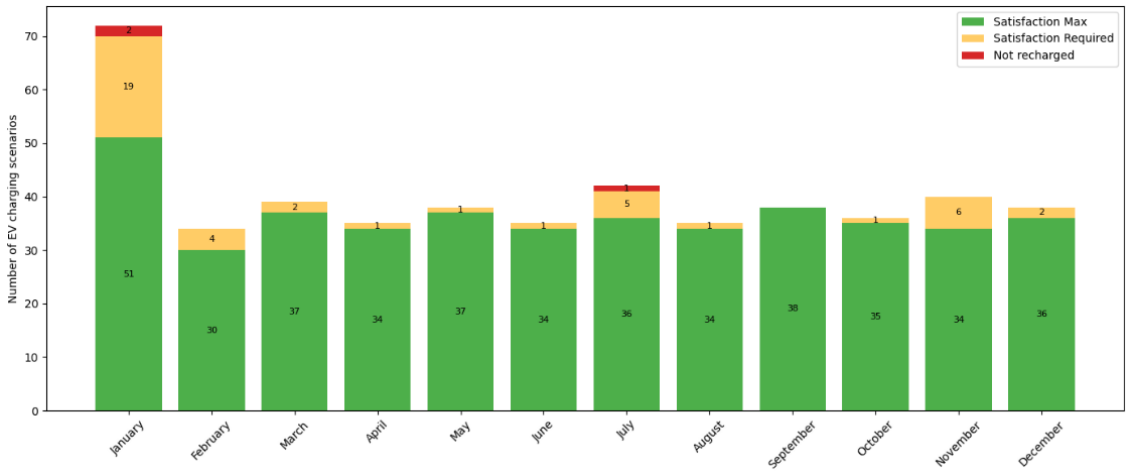

Figure 8. Charging scenarios of EVs with the satisfaction rate for two charging stations

Results of Pinch Power Analysis

The monthly profiles show a seasonal variability of residential load, higher in winter and lower during spring–summer, while the charging demand of EVs remains relatively stable. The integration of one or two charging stations adds a constant load, whose impact becomes significant in the sizing of HRES (**Figure 9**).

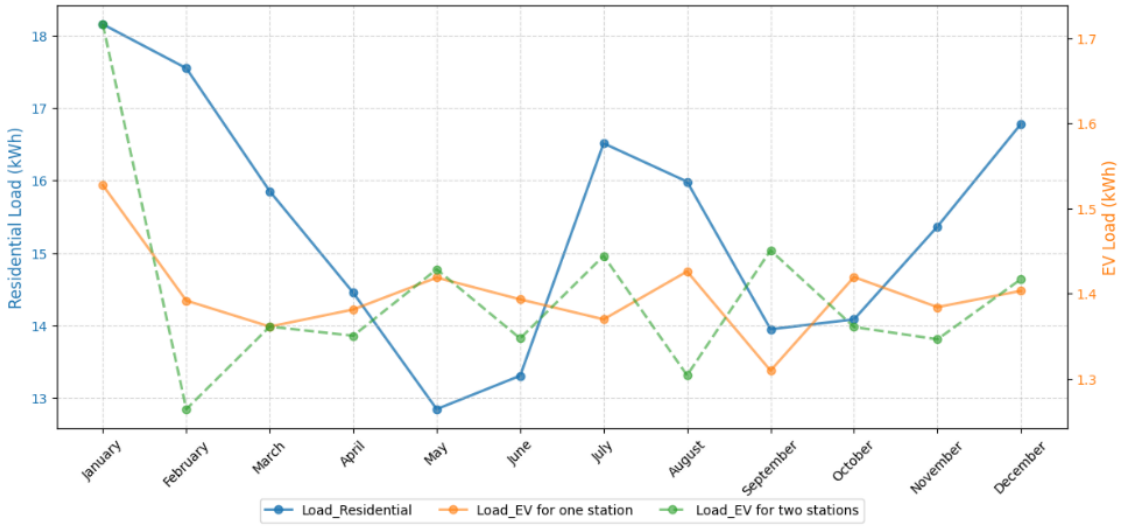

Figure 9. Residential and EV charging Load

The Pinch Power Analysis and strategy of EMS method is applied while respecting operational constraints to compare three energy consumption scenarios:

- **Scenario 1:** residential load only
- **Scenario 2:** residential load combined with EV charging
- **Scenario 3:** residential load combined with EV charging using two chargers

Step 1: Results of Daily-Based Preliminary Sizing and Energy Balance Optimisation. (**Figure 10**) illustrates the average 24h evolution, calculated over one year, of $E_{acc}(t)$ in the BESS before and after applying the Pinch Power Analysis approach.

The purpose is to determine the optimal sizing of energy systems (*N*pv, *Nw*, *Nbat*) and the operational constraints (E_{acc}^{min} and E_{acc}^{max}) for two energy configurations under these scenarios.

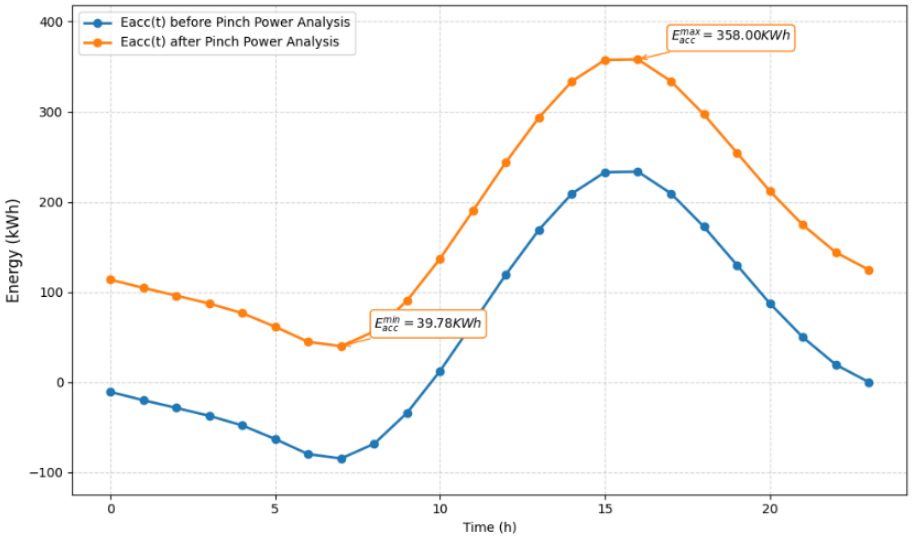

Figure 10. Eacc(t) in the BESS, averaged over a year on a 24-hour basis, for Configuration II under Scenario 2 for LPSP=1.54%

The evolution of $E_{acc}(t)$ over the 24-hour average (**Figure 11**)-(**Figure 12**) shows that the two curves corresponding to the scenarios overlap at the beginning of the day, which indicates that the $E_{acc}^{initial}$ is identical in both cases, since the residential load is active only.

EV charging begins in the evening, from 16:00 onward, causing a gradual divergence between the two curves, this results in an increase of approximately 15% in peak demand, reflected in both the E_{acc}^{min} *and* E_{acc}^{max} values of the accumulated energy in BESS. After the charging period, the two curves converge again, indicating that the impact of EV charging is concentrated exclusively in the evening time window.

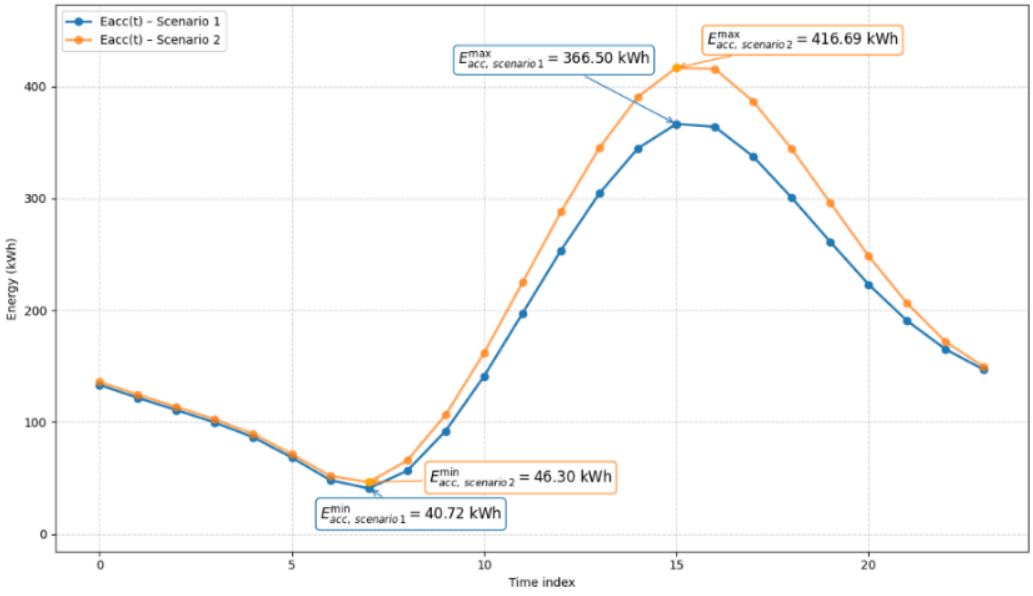

Figure 11. Eacc(t) in the BESS averaged over a year on a 24h basis, for Configuration I (scenario 1 and 2) after Pinch power analysis with 1% < *LPSP* < 2%

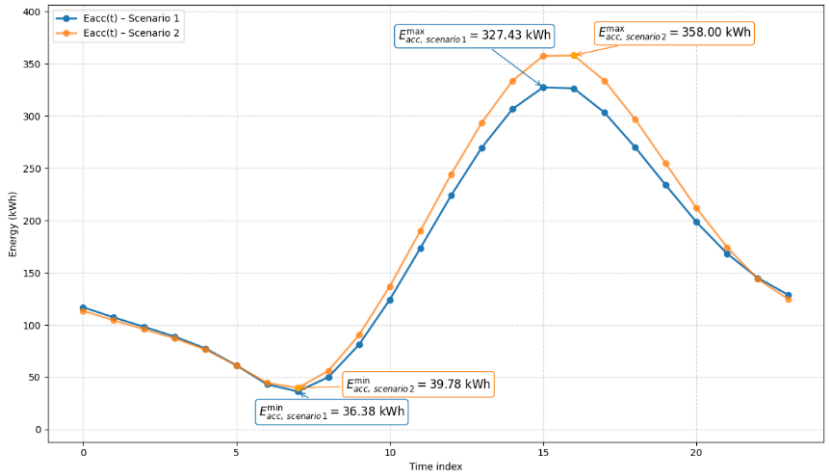

Figure 12. Eacc(t) in the BESS averaged over a year on a 24h basis, for Configuration II (scenario 1 and 2) after Pinch power analysis with 1% < *LPSP* < 2%

Step 2: Results of Hourly-Based Annual Verification with Operational Constraints. The tables below present the results obtained after validation, under operational constraints, of the sizing determined in Step 1, highlighting several fundamental relationships between sizing and the performance of hybrid systems. During this stage, the objective functions *LPSP*, *FEE*, and *EPSP* can be evaluated.

A significant reduction in *LPSP* reflects improved energy availability, inevitably requiring an increase in the capacity of PV panels and BESS.

For instance, in Configuration I, the decrease in *LPSP* from 11.85% to 1.95% in Scenario 1 (**Table 1**) is accompanied by an increase in the number of batteries from 19 to 28 units, and PV panels from 211 to 316.

This system expansion leads to a rise in the *LCOE* from 0.057 EUR/kWh to 0.083 EUR/kWh (**Table 5**), illustrating the economic trade-off associated with improved reliability.

Table 1. Optimal sizing results for Configuration I

Configuration I								
Scenario 1			Scenario 2			Scenario 3		
LPSP [%]	*Npv*	*Nbat*	*LPSP* [%]	*Npv*	*Nbat*	*LPSP* [%]	*Npv*	*Nbat*
11.85	211	19	11.5	230	22	11.78	231	22
7.67	239	21	7.58	260	24	7.87	261	24
5.33	259	23	5.33	282	26	5.16	284	27
3.86	274	25	3.94	298	28	4.17	299	28
3.19	285	26	3.23	310	29	2.77	325	30
1.95	316	28	1.86	343	32	1.37	365	34

Table 2. Optimal Power Converter Sizing Results for Configuration I

Configuration I					
Scenario 1		Scenario 2		Scenario 3	
Inverter Power Input [kW]	Rectifier Power Input [kW]	Inverter Power Input [kW]	Rectifier Power Input [kW]	Inverter Power Input [kW]	Rectifier Power Input [kW]
39.49	0	44.89	0	47.55	0
39.49	0	44.89	0	47.55	0
39.49	0	44.89	0	47.55	0
39.49	0	44.89	0	47.55	0
39.49	0	44.89	0	47.55	0
39.49	0	44.89	0	47.55	0

In Configuration II, a similar trend is observed (**Table 3**): in Scenario 1, the reduction of LPSP from 9.9% to 1.21% corresponds to an increase in the number of batteries from 18 to 25 units, while the LCOE remains stable at approximately 0.10 EUR/kWh (**Table 6**). The integration of WT enables the achievement of comparable reliability levels with a less heavily utilised energy storage capacity, reflecting the temporal complementarity effect between PV and WT.

Table 3. Optimal sizing results for Configuration II

Configuration II											
Scenario 1				Scenario 2				Scenario 3			
LPSP [%]	*Npv*	*Nw*	*Nbat*	*LPSP* [%]	*Npv*	*Nw*	*Nbat*	*LPSP* [%]	*Npv*	*Nw*	*Nbat*
9.9	136	1	18	9.9	155	1	20	9.99	155	1	20
6.02	159	1	20	6.03	180	1	22	6.15	181	1	22
4.34	174	1	21	4.08	197	1	24	4.24	197	1	24
3.28	185	1	22	3.14	208	1	25	3.28	209	1	25
2.75	194	1	22	--	--	--	--	--	--	--	--
1.21	227	1	25	1.54	239	1	28	1.69	240	1	28

Table 4. Optimal Power Converter Sizing Results for Configuration II

Configuration II					
Scenario 1		Scenario 2		Scenario 3	
Inverter Power Input[kW]	Rectifier Power Input [kW]	Inverter Power Input [kW]	Rectifier Power Input [kW]	Inverter Power Input [kW]	Rectifier Power Input [kW]
36.43	13.6	40.5	13.6	47.45	13.6
36.43	13.6	40.5	13.6	47.45	13.6
36.43	13.6	40.5	13.6	47.45	13.6
36.43	13.6	40.5	13.6	47.45	13.6
36.43	13.6	--	--	--	--
36.43	13.6	40.5	13.6	47.45	13.6

Furthermore, *EGR* (**Table 6**) increases as the *LPSP* decreases in Configuration II, rising from 64.39% to 75.12% (Scenario 1), indicating a growing share of PV production within a generally more reliable configuration.

The addition of wind power reveals a beneficial temporal complementarity that significantly reduces storage requirements: at an *LPSP* of 1.21% in Configuration II, the number of batteries needed is almost equivalent to that required at a higher LPSP of 3.86% in Configuration I (approximately 25 batteries, see **Table 1** and **Table 3**). This equivalence confirms the favourable effect of wind power in limiting storage needs for a given reliability level.

This complementarity is also reflected by *FEE* value, close to zero, corresponding to LPSP values between 5% and 10% in Configuration II, whereas it remains high in Configuration I (**Table 6**).

Moreover, the hybrid system in Configuration II achieves a better balance between production and demand, reducing unused energy surplus (*EPSP*) (**Table 6**), However, *EPSP* shows a slight decrease compared to Configuration I (**Table 5**) , which is mainly explained by the high penetration rate of solar renewable energy (*EGR*) in Configuration II. In other words, the strong solar contribution in this configuration helps stabilise overall system performance despite changes induced by integrating other resources or loads, thereby limiting reductions in *EPSP*.

Table 5. Techno-economic results for the configuration I

Configuration I								
Scenario 1			Scenario 2			Scenario 3		
FEE [%]	*LCOE* [EUR/kWh]	*EPSP* [%]	*FEE* [%]	*LCOE* [EUR/kWh]	*EPSP* [%]	*FEE* [%]	*LCOE* [EUR/kWh]	EPSP [%]
3.01	0.057	12.66	0	0.059	12.11	1.22	0.059	12.75
14.61	0.063	19.48	9.85	0.065	19.06	11.9	0.065	19.61
20.55	0.069	24	15.49	0.07	23.75	19.71	0.072	24.13
25.48	0.074	27.19	20.26	0.075	26.93	22.02	0.075	27.34
27.7	0.077	29.64	22.44	0.078	29.36	26.14	0.081	32.43
31.75	0.083	36.08	28.14	0.086	35.58	32.82	0.091	39.35

Table 6. Techno-economic results for configuration II

Configuration II											
Scenario 1				Scenario 2				Scenario 3			
FEE [%]	*LCOE* [EUR/kWh]	*EPSP* [%]	*EGR* [%]	*FEE* [%]	*LCOE* [EUR/kWh]	*EPSP* [%]	*EGR* [%]	*FEE* [%]	*LCOE* [EUR/kWh]	*EPSP* [%]	*EGR* [%]
0	0.094	10.99	64.39	0	0.091	10.78	67.34	0	0.091	10.83	67.34
0	0.1	16.47	67.89	0	0.097	16.25	70.54	0	0.097	16.67	70.65
0	0.1	20.25	69.83	0	0.1	20.01	72.38	0	0.10	20.11	72.38
1.39	0.1	22.9	71.1	0	0.1	22.48	73.45	1.91	0.10	22.84	73.54
6.24	0.1	25.17	72.07	--	--	--	--	--	--	--	--
21.15	0.11	32.65	75.12	12.66	0.11	29.28	76.07	14.84	0.11	29.59	76.14

The integration of EV results in a notable increase in energy and storage requirements, but its overall impact remains controlled and limited, with *EPSP* varying moderately between -0.55% and +3.37% depending on the configuration, reflecting the system's stability in response to this new demand (**Table 5** and **Table 6**).

The robust sizing of the BESS and the implemented management strategies help maintain *EPSP* levels close to those of scenarios without EVs. Furthermore, variations in the *LCOE* remain low after the integration of EV charging, in Configuration II (**Table 6**), and in Configuration I (**Table 5**), demonstrating the effectiveness of the EMS in economically adapting the system.

Thus, the system accommodates this additional load without significantly compromising its performance in terms of reliability and cost.

On an hourly daily dynamic, both configurations show charging predominantly concentrated during daylight hours when solar production is optimal, typically between 9 AM and 5–6 PM.

For Configuration II, the charging peaks $E_{\mathrm{BESS}}^{\mathrm{ch}}(t)$ reach high levels, sometimes exceeding 40 to 70 kWh/h around midday during seasons with strong sunlight (spring/summer), whereas Configuration I exhibit a slightly wider range, varying from 20 to 80 kWh/h, indicating greater variability in solar load. However, when demand persists and solar production wanes, significant discharges $E_{\mathrm{BESS}}^{\mathrm{disch}}(t)$ occur, reaching -30 to -40 kW/h in both Configurations II and I, mainly in autumn and winter, reflecting substantial reliance on batteries (**Figure 13**) and (**Figure 14**).

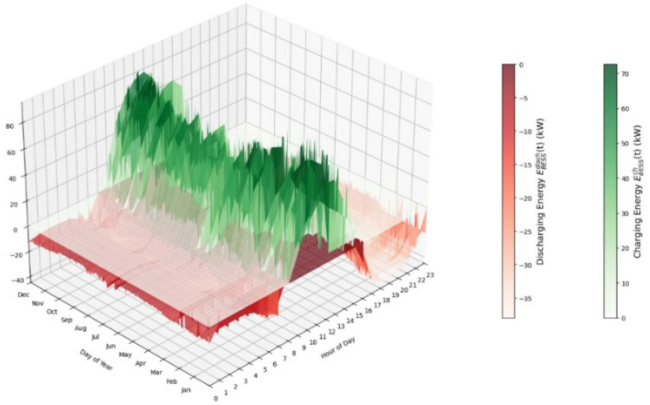

Figure 13. Yearly discharge profiles E_BESS^disch (t) and charge profiles E_BESS^ch (t) of the BESS in Configuration I under Scenario 2

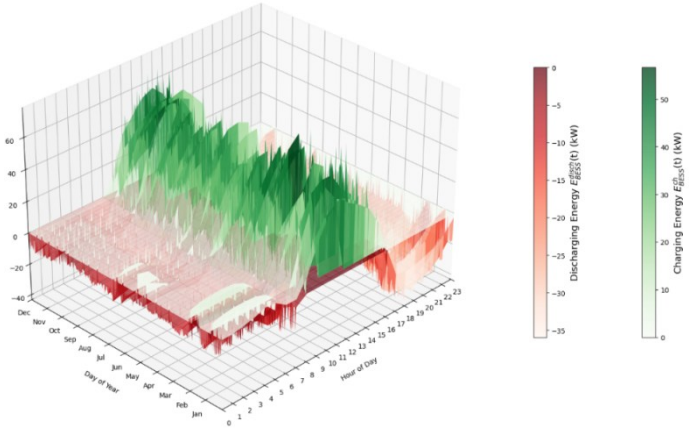

Figure 14. Yearly discharge profiles E_BESS^disch (t) and charge profiles E_BESS^ch (t) of the BESS in Configuration II under Scenario 2

During spring and summer, the system operates optimally, with overall demand generally lower (**Figure 9**) (around 15 to 17 kW/h), meanwhile, Configuration II benefits from a solar production average that increases significantly, reaching 465 to 536 kWh/day (**Figure 15**) and wind power generation in Configuration II remains low and consistent (on average ~140 kWh/day), sometimes dropping below 90 kWh/day, and contributes only moderately to recharging (**Figure 16**).

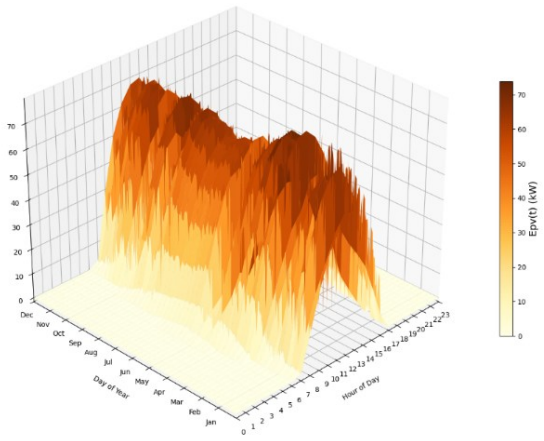

Figure 15. Yearly profiles of Epv(t), representing the solar energy generated in Configuration II under Scenario 2

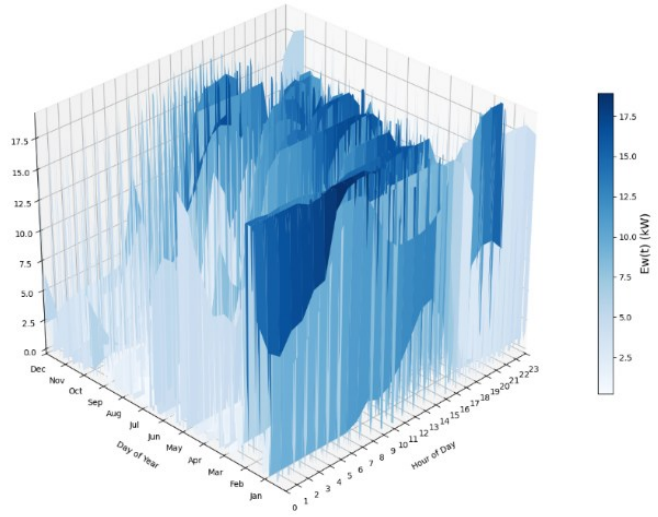

Figure 16. Yearly profiles of Ew(t), representing the wind energy generated in Configuration II under Scenario 2

Consequently, the SOC_{BESS} in Configuration II (**Figure 18**) mainly fluctuates between 40% and 80%, indicating that the batteries are often highly charged, with limited discharges. This results in higher charging levels of the BESS, close to but often below the demand, with more regular (~175 kWh/day on average) and elevated yet shallow discharge cycles generally ranging between -247 and -164 kWh/day (**Figure 14**), reflecting a cautious management strategy aimed at prolonging battery life. On days with exceptionally high solar production, excess energy may even occur if demand is low and the SOC_{BESS} approaches its maximum limit.

In Configuration I, the SOC_{BESS} also remains high (**Figure 17**), frequently above 45–70%, with fewer deep cycles, thereby limiting deep discharges (**Figure 13**). However, the more pronounced presence of solar peaks allows for fuller BESS charging and a more stable maximum *SOC* above 70%, reflecting a good match with variable summer demand.

In autumn and winter, with average demand (**Figure 9**) gradually increasing to approximately 15–18 kW/h and generally settling in winter—often above 18 kW/h, reaching up to 21 kW/h and solar production in Configuration II decreases (**Figure 15**) to an average level of around 372–490 kWh/day, partially offset by wind production (**Figure 16**) which rises to 104–334 kWh/day and remains relatively high in winter with notable peaks up to 356 kWh/day on windy days. This complementarity allows the SOC_{BESS} (**Figure 18**) to fluctuate between 30% and 80%, occasionally dropping to 10%, with significant discharge dynamics regularly reaching -314 and -187 kWh/day (**Figure 14**), particularly on days when reduced solar output is not compensated by wind (<100 kWh/day) and with charging energy of BESS sometimes (~260 kWh/day on average) close to or slightly below the demand. This indicates that solar production alone cannot cover consumption, resulting in increased reliance on discharges, while generally avoiding reaching the critical low threshold (SOC_{BESS} is often below 30%). However, in Configuration I, despite the high variability of solar production (peaks of >700 kWh/day on some days but also days with lower solar energy between 540 and 650 kWh/day), combined with relatively stable energy needs, the batteries undergo deep and frequent discharge cycles (**Figure 13**), et The SOC_{BESS} can then frequently drop to between 10% and 15% (**Figure 17**), with the daily maximum limited to 35–50%, imposing increased stress on the battery and posing a potential risk to its durability, particularly due to prolonged and frequent discharges.

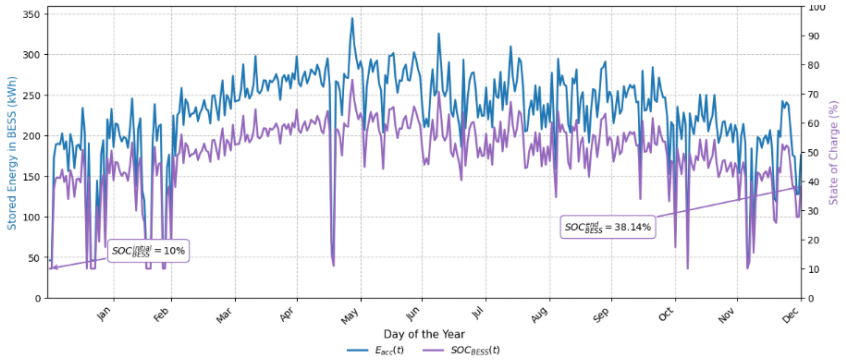

Figure 17. Yearly profiles of Eacc(t) and 〖SOC〗_BESS (t) for the BESS in Configuration I under Scenario 2

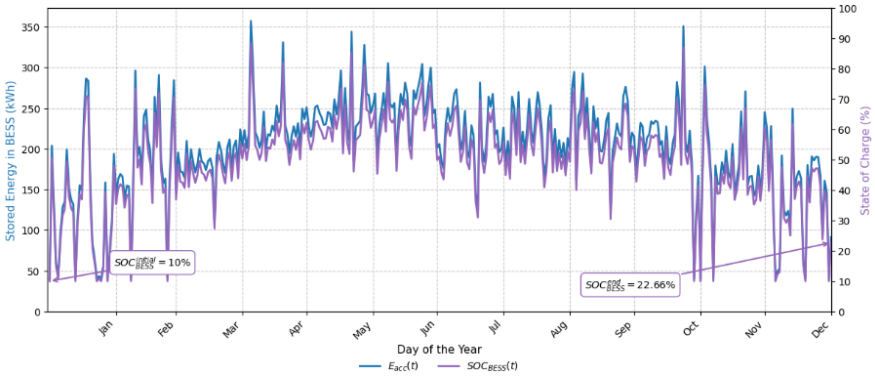

Figure 18. Yearly profiles of Eacc(t) and 〖SOC〗_BESS (t) for the BESS in Configuration II under Scenario 2

Thus, Configuration II offers better regulation of energy dynamics, thanks to the moderating contribution of wind power in winter and more balanced battery cycles, promoting the long-term health of the batteries. Although Configuration I performs well in summer with higher solar production, it presents an increased risk of deep discharges and taxing battery cycles during the cold season, due to lesser wind energy complementarity and greater solar variability.

The integration of the sale of 20% of excess energy eq. (23) (in accordance with Law 82-21 on self-production of electricity applied in Morocco) at prices equivalent to %SALE = 40%, 50%, and 60% of the reference *LCOE* (**Table 5** and **Table 6**) results in a significant reduction of *LCOE* for all studied systems, giving the $LCOE_{SALE}$ values shown in **Table 7** and **Table 8**. This decrease is proportional to the applied sale price: the higher the price, the greater the reduction.

Table 7. Results of the new LCOE values after selling excess energy for Configuration I

Configuration I									
	Scenario 1			Scenario 2			Scenario 3		
LPSP [%]	%SALE =40%	%SALE =50%	%SALE =60%	%SALE =40%	%SALE =50%	%SALE =60%	%SALE =40%	%SALE =50%	%SALE =60%
11.85	0.0522	0.051	0.0498	0.0542	0.053	0.0518	0.0543	0.0531	0.0519
7.67	0.0574	0.0559	0.0544	0.0591	0.0576	0.0561	0.0592	0.0577	0.0561
5.33	0.0606	0.0585	0.0564	0.0621	0.06	0.0579	0.0636	0.0614	0.0592
3.86	0.0634	0.0607	0.058	0.0646	0.0619	0.0592	0.0645	0.0617	0.059
3.19	0.0644	0.0612	0.0581	0.0655	0.0623	0.0591	0.0659	0.0621	0.0583
1.95	0.0652	0.0606	0.0559	0.0674	0.0628	0.0581	0.0682	0.0623	0.0564

Table 8. Results of the new LCOE values after selling excess energy for Configuration II

Configuration II									
	Scenario 1			Scenario 2			Scenario 3		
LPSP [%]	%SALE =40%	%SALE =50%	%SALE =60%	%SALE =40%	%SALE =50%	%SALE =60%	%SALE =40%	%SALE =50%	%SALE =60%
9.9	0.0865	0.0846	0.0827	0.0841	0.0822	0.0804	0.0842	0.0823	0.0805
6.02	0.0911	0.0888	0.0866	0.0884	0.0862	0.0840	0.0886	0.0863	0.0841
4.34	0.0934	0.0909	0.0883	0.0923	0.0898	0.0873	0.0923	0.0898	0.0874
3.28	0.0942	0.0911	0.088	0.093	0.09	0.087	0.0929	0.0899	0.0869
2.75	0.0932	0.0897	0.0861	--	--	--	--	--	--
1.21	0.0939	0.0883	0.0827	0.0943	0.0897	0.0851	0.0942	0.0895	0.0848

The analysis indicates that the economic impact of valorising excess energy depends on the *LPSP* level. For low *LPSP*, the sale of surplus energy allows a further reduction in cost, as initial values of *LCOE*s remain high compared to systems with high *LPSP*. Moreover, for the same sale price, $LCOE_{SALE}$ remains very close regardless of *LPSP*, suggesting that valorisation of excess energy reduces the cost gap between systems with low and high *LPSP*, thereby mitigating the impact of oversizing and enhancing the economic viability of renewable systems. Finally, as the percentage of energy sold increases, this convergence of $LCOE_{SALE}$ values becomes even more pronounced, strongly reducing the relative effect of *LPSP* on the final cost.

Validation by Homer Pro software. The results obtained with Homer Pro (**Table 9** and **Table 10**), using the equipment sizing derived from des **Table 1** and **Table 3** initially corresponding to an *LPSP* of approximately 1%, generally confirms the reliability and consistency of the modelled systems. Although the *LPSP* calculated by Homer Pro shows some variation, ranging from 0.9% to 1.74%, these values remain low and close to the initial target, thus ensuring satisfactory energy continuity.

Furthermore, other key indicators such as *EPSP*, *LCOE*, and *FEE* present results consistent with those in **Table 5** and **Table 6**, reflecting effective energy production management, maintained reliability, and solid economic control. The stable numbers of PV panels, WT, and batteries between the two sets of results further reinforce this validation, demonstrating that the initial sizing meets the system requirements within Homer Pro.

Table 9. Optimal sizing and techno-economic results for configuration I and scenario 2 were obtained using Homer Pro software

Configuration I								
	LPSP [%]	*Npv*	*Nbat*	*FEE* [%]	*LCOE* [EUR/kWh]	*EPSP* [%]	Inverter Power Input[kW]	Rectifier Power Input [kW]
Scenario 1	1.74	315	28	28.53	0.085	36.5	38.7	0
Scenario 2	1.6	342	32	24.51	0.087	36.1	44	0

Table 10. Optimal sizing and techno-economic results for configuration II and scenario 2 were obtained using Homer Pro software

Configuration II										
	LPSP [%]	*Npv*	*Nw*	*Nbat*	*FEE* [%]	*LCOE* [EUR/kWh]	*EPSP* [%]	*EGR* [%]	Inverter Power Input [kW]	Rectifier Power Input [kW]
Scenario 1	0.9	227	1	25	22.41	0.11	33	75.9	35.7	13.3
Scenario 2	1.24	239	1	28	16.15	0.11	29.9	76.8	39.7	13.3

CONCLUSION

This study demonstrates that a structured two-step optimisation framework, combining Pinch Power Analysis and integrated EMS, enables a robust sizing of a HRES incorporating EV charging, while generating EV charging profiles and managing techno-economic trade-offs.

The main scientific contribution lies in the integration of a simplified daily pre-sizing (24 h) with an annual hourly validation, reducing computational complexity while ensuring system reliability over 8760 hours.

From a practical perspective, these results provide a decision-making framework for the design of hybrid systems. Improving reliability (reducing *LPSP*) incurs measurable costs, and the integration of wind power allows achieving a lower *LPSP* (1.21 %) with a stable *LCOE* of approximately 0.10 EUR/kWh for *LPSP* > 10 %, requiring only 25 batteries. This number is nearly equivalent to that required for a higher *LPSP* of 3.86 % in the PV/BESS configuration, highlighting the role of WT–PV complementarity in reducing storage requirements for a given reliability level.

This complementarity is also reflected in the *FEE* value, which remains close to zero for *LPSP* between 5 % and 10 %, whereas it is higher in the PV/BESS configuration. Moreover, the SOC_{BESS} predominantly remains between 40 % and 80 % in the WT/PV/BESS configuration, while deeper discharges reaching 10–15 % are observed in the PV/BESS configuration, particularly during winter. Thus, although the PV/BESS configuration exhibits a slightly lower cost of energy, the addition of wind power improves seasonal stability and reduces storage stress.

The integration of EVs increases energy and storage requirements, but its impact remains controlled: reliability and cost indicators vary only slightly, demonstrating the effectiveness of the EMS in the economic and operational adaptation of the system. Validation with HOMER confirms the consistency of the sizing and the stability of the achieved performance.

Certain limitations should be noted: the analysis relies on deterministic annual climate profiles. Future research could incorporate stochastic scenarios for renewable generation and charging behaviour, as well as a more detailed economic sensitivity analysis, including investment costs (residential, commercial, utility scale) and a wider diversity of energy resources (hydrogen, hydropower).

As a continuation of this work, several research perspectives can be explored. In particular, a detailed techno-economic analysis should be conducted to assess the integration capacity of renewable energy systems into medium-voltage (MV) and low-voltage (LV) networks, considering power flow constraints, power quality, and dynamic load management. Furthermore, the implementation of advanced energy dispatch strategies is essential to optimise generation, minimise operational costs, and ensure system reliability.

NOMENCLATURE

Symbols

LCOE	Levelized Cost of Energy	[USD/kWh]
LPSP	Loss of Power Supply Probability	[%]
EPSP	Excess Power Supply Probability	[%]
FEE	Final Excess Energy	[%]
EGR	Energy Generation Ratio	[%]
BECR	Battery Energy Charging Ratio	[%]
RDR	Recovered Driving Range	[km]

Abbreviations

BESS	Battery Energy Storage System
EMS	Energy Management System
ESCEA	Electric System Cascade Extended Analysis
EV	Electric Vehicle
GA	Genetic Algorithm
GA-PSO	Hybrid Genetic Algorithm–Particle Swarm Optimization
HOMER Pro	Hybrid Optimization of Multiple Energy Resources (Professional version)
LCA	Life Cycle Assessment
MOPSO	Multi-Objective Particle Swarm Optimization
NREL	National Renewable Energy Laboratory
PSO	Particle Swarm Optimization
PV	Photovoltaic
WT	Wind Turbine
BOS	Balance of System

APPENDIX

Table 11. EV parking behaviour and characteristics

ID_{EV}	$Cbat_{\mathrm{EV}}^{\mathrm{ID_{EV}}}$	$RDR_{\mathrm{max}}^{\mathrm{ID_{EV}}}$	$\mathrm{Charg}_{\mathrm{pow\_EV}}^{\mathrm{max}}$	$RDR_{\mathrm{target}}^{ID_{\mathrm{EV}}}$	t_{arrival}[h]	t_{arrival}[min]	t_{depart}[h]	t_{depart}[min]
1	38.4	270	6.6	15	16	20	23	30
2	37.9	305	7.4	20	16	40	23	30
3	64.8	460	7.4	16	17	20	23	30
4	50	357	7.4	17	17	30	23	30
5	32.3	260	7.2	12	17	30	23	30
6	46	359	7.4	19	18	10	23	30
7	64.8	460	7.4	25	18	30	23	30
8	38.4	270	6.6	12	18	30	23	30
9	52	395	7.4	13	18	40	23	30
10	54	406	7.4	15.6	19	0	23	30
11	37.9	305	7.4	18	19	30	23	30
12	32.3	260	7.2	13	19	40	23	30
13	50	357	7.4	14.5	19	40	23	30
14	52	395	7.4	19.5	20	0	23	30
15	46	359	7.4	20	20	0	23	30

Table 12. Characteristics of HRES

PV module DATA	
Peak power rating	327 W
Maximum Power Point Voltage	54.7 V
Maximum Power Point Current	5.98 A
Open-Circuit Voltage	64.9 V
Short-circuit current	6.46 A
Area	1.63 m^2
Module efficiency (η_{ref})	20.4 %
Normal operating cell temperature (T_{NOCT})	45 C
Temperature coefficient of efficiency (β)	-0.04 %/ K
Temperature at rated efficiency (Tref)	25 °C
Solar radiation at T_{NOCT} (I_{NOCT})	800 W/m^2
Cost per unit	124 EUR
BOS cost	35% of PV system costs
Installation cost	10% of the overall project cost
O&M cost [USD/kW-yr]	1% of the initial cost of the installation

Wind energy system	
Rated power (Pn)	20 kW
Cut in speed ($v_{\text{cut\_in}}$)	2.75 m/s
Cut out speed ($v_{\text{cut\_out}}$)	20 m/s
Rated speed (v_{nom})	12 m/s
Rotor diameter (r)	12 m
gearbox efficiency (η_{gearbox})	98 %
generator efficiency ($\eta_{\text{generator}}$)	98 %
Cost per unity	49,680 EUR
BOS cost	40% of the WT system cost
O&M cost [USD/kW-yr]	1% of the initial cost of the installation
Battery Energy Storage System (BESS)	
Battery capacity ($Cbat$)	300 Ah
Battery voltage	48 V
Courant de Charge Max.	200 A
Courant de Décharge Max.	200 A
Depth of discharge (DOD)	90%
Maximum state of charge (*SOC* max)	90%
Cost per unity	1902 EUR
Cost of bidirectional inverter	169 EUR
BOS cost	35% of BESS cost
O&M cost [USD/kW-yr]	1% of the initial cost of the installation

REFERENCES

1. Nagapurkar, P., Smith, J. D., Techno-economic Optimization and Environmental Life Cycle Assessment (LCA) of Microgrids Located in the US Using Genetic Algorithm, Energy Conversion and Management, Vol. 181, pp 272–291, 2019, https://doi.org/10.1016/j.enconman.2018.11.072.
2. Dadjiogou, K. Z., Ajavon, A. S. A., Bokovi, Y., Energy Flow Management in a Smart Microgrid Based on Photovoltaic Energy Supplying Multiple Loads, *Journal of Sustainable Development of Energy, Water and Environment Systems*, Vol. 12, No. 1, 1110473, 2024, https://doi.org/10.13044/j.sdewes.d11.0473.
3. Ma, J., Yuan, X., Techno-economic Optimization of Hybrid Solar System with Energy Storage for Increasing the Energy Independence in Green Buildings, *Journal of Energy Storage*, Vol. 61, 106642, 2023, https://doi.org/10.1016/j.est.2023.106642.
4. Das, B. K., Hasan, M., Rashid, F., Optimal Sizing of a Grid-Independent PV/Diesel/Pump-Hydro Hybrid System: A Case Study in Bangladesh, *Sustainable Energy Technologies and Assessments*, Vol. 44, 100997, 2021, https://doi.org/10.1016/j.seta.2021.100997.
5. Mulumba, A., Ngila, J.C., Farzaneh, H., Techno-Economic Analysis and Dynamic Power Simulation of a Hybrid Solar-Wind-Battery-Flywheel System for Off-Grid Power Supply in Remote Areas in Kenya, *Energy Conversion and Management: X*, Vol. 18, 100381, 2023, https://doi.org/10.1016/j.ecmx.2023.100381.
6. Xu, C., Ke, Y., Li, Y., Chu, H., Wu, Y., Data-Driven Configuration Optimization of an Off-Grid Wind/PV/Hydrogen System Based on Modified NSGA-II and CRITIC-TOPSIS, *Energy Conversion and Management*, Vol. 215, 112892, 2020, https://doi.org/10.1016/j.enconman.2020.112892.

7. Das, P., Das, B. K., Rahman, M., Hassan, R., Evaluating the Prospect of Utilizing Excess Energy and Creating Employments from a Hybrid Energy System Meeting Electricity and Freshwater Demands Using Multi-Objective Evolutionary Algorithms, *Energy*, Vol. 238, 121860, 2022, https://doi.org/10.1016/j.energy.2021.121860.
8. Ghorbani, N., Kasaeian, A., Toopshekan, A., Bahrami, L., Maghami, A., Optimizing a Hybrid Wind-PV-Battery System Using GA-PSO and MOPSO for Reducing Cost and Increasing Reliability, *Energy*, Vol. 154, pp 581–591, 2018, https://doi.org/10.1016/j.energy.2017.12.057.
9. Zereg, H., Bouzgou, H., Forecast-Integrated Techno-Economic Optimization of Off-Grid Hybrid Renewable System in Hyper-Arid Regions: Application to Tamanrasset, Algeria, *Energy*, Vol. 334, 137468, 2025, https://doi.org/10.1016/j.energy.2025.137468.
10. Al Dawsari, S., Anayi, F., Packianather M., Techno-Economic Analysis of Hybrid Renewable Energy Systems for Cost Reduction and Reliability Improvement Using Dwarf Mongoose Optimization Algorithm, *Energy*, Vol. 313, 133653, 2024, https://doi.org/10.1016/j.energy.2024.133653.
11. Roumi, S., Stewart, R., Karkoodi, S., Parvin, M., Analysis of Optimal Energy Supply in the Commercial Buildings: A Herpetarium, *Journal of Sustainable Development of Energy, Water and Environment Systems*, Vol. 10, No. 2, 1090394, 2022, https://doi.org/10.13044/j.sdewes.d9.0394.
12. Mehrpooya, M., Sharifzadeh, M. M. M., A novel integration of oxy-fuel cycle, high temperature solar cycle and LNG cold recovery – energy and exergy analysis, *Applied Thermal Engineering*, Vol. 114, pp 1090-1104, 2017, https://doi.org/10.1016/j.applthermaleng.2016.11.163.
13. Mohammed, C. et al., Extended Method for the Sizing, Energy Management, and Techno-Economic Optimization of Autonomous Solar Photovoltaic/Battery Systems: Experimental Validation and Analysis, *Energy Conversion and Management*, Vol. 270, 116267, 2022, https://doi.org/10.1016/j.enconman.2022.116267.
14. Chennaif, M., Zahboune, H., Elhafyani, M., and Zouggar, S., Electric System Cascade Extended Analysis for Optimal Sizing of an Autonomous Hybrid CSP/PV/Wind System with Battery Energy Storage System and Thermal Energy Storage, *Energy*, Vol. 227, pp 120444, 2021, https://doi.org/10.1016/j.energy.2021.120444.
15. Chennaif, M., Maaouane, M., Zahboune, H., Elhafyani, M., Zouggar, S., Tri-Objective Techno-Economic Sizing Optimization of Off-Grid and On-Grid Renewable Energy Systems Using Electric System Cascade Extended Analysis and System Advisor Model, Applied *Energy*, Vol. 305, pp 117844, 2022, https://doi.org/10.1016/j.apenergy.2021.117844.
16. Mohammed, C., Hassan, Z., Mohamed Larbi, E., Smail, Z., Jalal, B., Optimal Sizing of a Concentrated Solar Power System Powering an Autonomous Water Pumping System Using the Modified Electric Systems Cascade Analysis, *Materials Today: Proceedings*, Vol. 45, pp 7747–7751, 2021, https://doi.org/10.1016/j.matpr.2021.03.432.
17. Zahboune, H., Zouggar, S., Krajacic, G., Varbanov, P. S., Elhafyani, M., and Ziani, E., Optimal Hybrid Renewable Energy Design in Autonomous System Using Modified Electric System Cascade Analysis and Homer Software, *Energy Conversion and Management*, Vol. 126, No. 1, pp 909–922, 2016, https://doi.org/10.1016/j.enconman.2016.08.061.
18. Zahboune, H. et al., Modified Electric System Cascade Analysis for Optimal Sizing of an Autonomous Hybrid Energy System, *Energy*, Vol. 116, pp 1374–1384, 2016, https://doi.org/10.1016/j.energy.2016.07.101.
19. Soykan, G., Er, G., Canakoglu, E., Optimal Sizing of an Isolated Microgrid with Electric Vehicles Using Stochastic Programming, *Sustainable Energy, Grids and Networks*, Vol. 32, pp 100850, 2022, https://doi.org/10.1016/j.segan.2022.100850.

20. Natarajan, S., Rajan Singaravel, M. M., Alsenani, T. R., Optimal Sizing of Solar PV-Wind Systems, Battery Storage, and EV Charging Infrastructure for Efficient Energy Management in Large-Scale Commercial Buildings, *Applied Energy*, Vol. 402, 126865, 2025, https://doi.org/10.1016/j.apenergy.2025.126865.
21. Fachrizal, R., Shepero, M., Åberg, M., Munkhammar, J., Optimal PV-EV Sizing at Solar Powered Workplace Charging Stations with Smart Charging Schemes Considering Self-Consumption and Self-Sufficiency Balance, *Applied Energy*, Vol. 307, No. 5, 118139, 2022, https://doi.org/10.1016/j.apenergy.2021.118139.
22. Direya, R., Khatib, T., Simplified Python Models for Photovoltaic-Based Charging Stations for Electric Vehicles Considering Technical, Economic, and Environmental Aspects, World Electric Vehicle Journal, Vol. 14, No. 4, 2023, https://doi.org/10.3390/wevj14040103.
23. Jaganath, M. M., Ray, S., Choudhury, N. B. D., Eco-Friendly Microgrid Carport Charging Station for Electric Vehicles (EVs), *e-Prime - Adv. Electr. Eng. Electron. Energy*, Vol. 5, No. 4, 100196, 2023, https://doi.org/10.1016/j.prime.2023.100196.
24. Blonsky, M., Munankarmi, P., Balamurugan, S., Incorporating Residential Smart Electric Vehicle Charging in Home Energy Management Systems: Preprint, (Technical) Report, NREL, USA, 2021, https://doi.org/10.1109/GreenTech48523.2021.00039.
25. Kouka, K., Masmoudi, A., Abdelkafi, A., Krichen, L., Dynamic Energy Management of an Electric Vehicle Charging Station Using Photovoltaic Power, *Sustainable Energy, Grids and Networks*, Vol. 24, 100402, 2020, https://doi.org/10.1016/j.segan.2020.100402.
26. Iqbal, M. N., Bhatti, A. R., Farhan, M., Butt, A. D., Optimizing the Design of Hybrid Renewable Energy Systems Considering Electric Vehicle Loading, *Electric Power Systems Research*, Vol. 252, 112452, 2026, https://doi.org/10.1016/j.epsr.2025.112452.

Paper submitted: 07.09.2025
Paper revised: 20.04.2026
Paper accepted: 23.04.2026